Journal of Engineering Mechanics. Submitted May 20, 2011; accepted September 21, 2012;
posted ahead of print September 23, 2012. doi:10.1061/(ASCE)EM.1943-7889.0000553

Effect of torch angle on arc properties and weld pool shape in stationary GTAW

S. Parvez[1], M. Abid[2], D. H. Nash[3], H. Fawad[4] and A. Galloway[5]

[1]Faculty of Mechanical Engineering, GIK Institute, Topi, Pakistan

shahidp@giki.edu.pk

[2]Faculty of Mechanical Engineering, GIK Institute, Topi, Pakistan

abid@giki.edu.pk

[3]Department of Mechanical Engineering, Strathclyde University, Glasgow, UK

d.nash@strath.ac.uk

[4]Faculty of Mechanical Engineering, GIK Institute, Topi, Pakistan

hfawad@giki.edu.pk

[5]Department of Mechanical Engineering, Strathclyde University, Glasgow, UK

alex.galloway@strath.ac.uk

Corresponding author address

Faculty of Mechanical Engineering,

GIK Institute, Topi, Pakistan

abid@giki.edu.pk

Ph: +92 938 271858

Fax: +92 938 271889

Journal of Engineering Mechanics. Submitted May 20, 2011; accepted September 21, 2012; posted ahead of print September 23, 2012. doi:10.1061/(ASCE)EM.1943-7889.0000553

Abstract

In this paper, a three dimensional numerical simulation is performed on a stationary arc to study the effect of torch angle in gas tungsten arc welding (GTAW) of SS304 stainless steel. A comparison has been made to investigate 90^o and 70^o torch angles and analyze the effect on arc and weld pool shape. Current density, heat flux and gas shear stress are calculated in the arc region and are used as input to the workpiece to determine the weld pool. Buoyancy and Marangoni shear also affect the weld pool shape and are taken into account. The computed and experimental results are observed symmetric for 90^o torch angle. For 70^o torch angle, current density and hence the heat flux due to electron contribution is found the maximum behind and heat flux due to conduction and convection is found the maximum ahead of the electrode tip in the welding direction. This makes the maximum of total heat flux symmetric along the arc center. Heat flux due to conduction and convection decreases as the torch angle decreases resulting in a shallow weld pool. The non-symmetric "w" shaped weld pool is developed by the combined effect of the gas shear and Marangoni convection. It is found that for 70^o torch angle, the weld pool becomes non-symmetric, shallow and wide ahead of the electrode tip in the welding direction. The numerical weld pool shapes are verified through experiments.

Keywords: TIG welding, gas tungsten arc welding, numerical simulation of GTAW, torch angle, asymmetric weld pool, non-symmetric weld pool.

Journal of Engineering Mechanics. Submitted May 20, 2011; accepted September 21, 2012;
posted ahead of print September 23, 2012. doi:10.1061/(ASCE)EM.1943-7889.0000553

1 Introduction

Gas tungsten arc welding is a metal joining process in which an arc is formed between a non-consumable tungsten electrode and the workpiece. Argon is commonly used as a shielding gas and is fed through the torch nozzle to shield the electrode and molten weld pool. Many researchers developed two dimensional GTAW models with 90^o torch angle to study the arc and weld pool shape axisymmetrically. Quigley (Quigley et al., 1973) explored different heat transfer mechanisms i.e. conduction, convection, radiation, electron potential energy, electron thermal energy and anode fall. On the basis of heat balance, he determined the contribution of different heat transfer mechanisms to the workpiece. Zhu (Zhu et al., 1995) developed a mathematical model based on a unified treatment of the free burning arc-electrode system to determine the water cooled copper anode temperature. A unified mathematical model for stationary tungsten inert gas (TIG) welding process is developed by Tanaka (Tanaka et al., 2002) to analyze the tungsten cathode, the arc plasma and the weld pool. Sansonnens (Sansonnens et al., 2000) treated the arc and electrode sheath regions as a continuum to determine the thickness of the non-equilibrium region near the electrodes. Fenggui (Lu et al., 2004) used an FEM approach to study the interaction between the arc and weld pool. More recent work by Hua-yun (yun Du et al., 2009) used a two dimensional axisymmetric model to study the temperatures profiles, velocities, electric potential and current density distribution by changing the welding current, shielding gas flow rate, arc length and the type of shielding gas. Gleizes (Gleizes et al., 1997) investigated the effect of workpiece material on temperatures. In the weld pool studies, Kim and Na (Kim and Na, 1998) established a computational model to study heat transfer, fluid flow and phase change in pulsed current GTAW. A boundary-fitted coordinate system is used to precisely describe the curved fusion zone. The transient behavior of weld pool shape with deformed surface is investigated in reference (Thompson and Szekely, 1989). A mathematical model is governed in reference (Kanouff, 1992) to study the weld pool by considering the effect of Marangoni, Lorentz and buoyancy forces. A more detailed study on the Marangoni shear is presented in reference (Choo et al., 1992) which concludes that the thermocapillary flow can produce

Journal of Engineering Mechanics. Submitted May 20, 2011; accepted September 21, 2012;
posted ahead of print September 23, 2012. doi:10.1061/(ASCE)EM.1943-7889.0000553

high surface velocities and the precise relationship between the temperature and surface tension become less important. In a three dimensional study, Speckhofer and Schmidt investigated heat transfer and fluid flow in a magnetically deflected arc (Speckhofer and Schmidt, 1996). The same magnetically deflected arc is studied in reference (Gonzalez et al., 2005) which considered a unified model of the arc and anode. Li and Wu carried out a three dimensional model to describe the heat transfer and fluid flow in the interfacial region between arc and weld pool (Li and Wu, 1997).

All the studies cited above consider stationary, axisymmetric two dimensional models with normal (90^o) torch angle. However, the torch is not always normal to the workpiece and can be set to some optimum angle less than 90^o. The 70^o torch angle suggested in reference (Miller, 2008) is compared with the 90^o torch angle to investigate the arc properties and weld pool shape in stationary GTAW of SS304 stainless steel. The torch angle and other welding parameters are assumed to remain constant during the two second welding time. The objective is to implement a novel simulation methodology to predict the development of the arc and weld pool shape with tilted torch. using ANSYS CFX®. Furthermore; the temperature, current density, heat flux and gas shear stress are analyzed for the arc and the electromagnetic, buoyancy, and Marangoni forces are investigated in the weld pool. Surface deformation is not considered in the analysis. The computed weld pool shapes are compared with the experimental results and are found in good agreement.

2 Numerical Simulation

The three-dimensional, stationary gas tungsten arc welding process is analyzed using the computer software program, ANSYS CFX®. The software package is based on finite volume method and uses Navier-Stokes and Maxwell equations to simulate the arc welding phenomena. The governing equations are given in reference (ANSYS, 2010) and are therefore not presented in this paper. Following assumptions are made for the arc and weld pool analyses;

Journal of Engineering Mechanics. Submitted May 20, 2011; accepted September 21, 2012;
posted ahead of print September 23, 2012. doi:10.1061/(ASCE)EM.1943-7889.0000553

1. The arc is in local thermodynamic equilibrium (LTE).

2. The arc is stationary and is in steady state.

3. The computational domain is in planar symmetry.

4. The variable length of the electrode tip surrounded by the plasma is the same for 90^o and 70^o electrode angles.

5. The fluid motion is laminar.

6. The density variation is very small with temperature, therefore Boussinesq approximation is used.

7. Current density, gas shear and heat flux are determined under the assumption of the steady state arc.

2.1 The Arc

The computational domains for 90^o and 70^o torch angles are shown in figure 1. With 70^o torch angle, the computational domain becomes planar symmetric. In all studies presented herein, a direct current (DC) arc is used with an Argon flow of 14 liter/min at atmospheric pressure. The electrode composition is thoriated tungsten of diameter 3.2mm, arc length is 2mm and welding current is 130A. Extensive heat is generated by ohmic heating caused by the potential difference between the anode and cathode. Electromagnetic hydrodynamic model is used to simulate the phenomena. The $k-\varepsilon$ model is employed as described in reference (Gleizes et al., 2005). Argon is frequently used as a shielding gas in GTAW which becomes electrically conductive at a temperature greater than 7000K. Numerical testing revealed that a temperature of 12000K is suitable to achieve a sustainable ohmic heating, thus simulating the initiation of the arc is achieved by applying a heat source. The heat source is then removed when the required temperature is achieved. Temperature dependent properties of Argon are used given in reference (Murphy and Arundell, 1994).

Journal of Engineering Mechanics. Submitted May 20, 2011; accepted September 21, 2012;
posted ahead of print September 23, 2012. doi:10.1061/(ASCE)EM.1943-7889.0000553

More than 60% heat transfer to the anode surface takes place due to the electron contribution (Wu and Gao, 2002). Some authors reported that more than 80% heat transfer can be achieved (Ferjutz and Davis, 1993). Heat fluxes due to conduction and convection, electron potential energy, electron thermal energy and anode fall are modeled as given in equation 1 and are applied on the workpiece to simulate the weld pool. The energy absorbed by the electron is $j\phi$. Where j is the current density distribution on the workpiece surface. Electrons are traveling from the hot plasma to the workpiece surface carrying heat and current with them. This phenomenon heats the workpiece surface. The rate of electron energy transport is given by jV_{th}. Anode fall is a very thin non-equilibrium layer in front of the anode where a negative space charge is formed and voltage drop occurs. There is a negative space charge on the workpiece surface, which results a cloud of positively charged ions in the sheath region to strike the workpiece surface. This increases the temperature of the workpiece and is given by jV_a. Total heat flux to the anode is given by:

$$F = F_c + j(\phi + V_a + V_{th}) + F_R \tag{1}$$

The values of ϕ, V_a and V_{th} are taken from reference (Quigley et al., 1973). F_r is the radiation flux to the anode. The effect of radiation on the anode temperature is small (1.2%) and is neglected (Quigley et al., 1973).

2.2 The weld pool

The arc and weld pool are solved separately. Heat flux, current flux and gas shear stress are determined from the steady state are applied on the weld pool surface to analyze the weld pool shape transiently after two seconds. This approach is adopted from reference (Goodarzi et al., 1998). It is assumed that the variation in density of the liquid SS304 is small, therefore Boussinesq approximation is used to calculate the buoyancy driven convection. To simulate the liquid and solid phases of the workpiece, both the regions are treated as a single domain as used by Lu in reference (Lu et al., 2006). Large viscosity is given where the temperature is equal or less than the solidus temperature and actual

Journal of Engineering Mechanics. Submitted May 20, 2011; accepted September 21, 2012;
posted ahead of print September 23, 2012. doi:10.1061/(ASCE)EM.1943-7889.0000553

viscosity is defined where the temperature is above the solidus. All other properties are temperature dependent and are taken from reference (Leibowitz, 1976). The material of the workpiece is SS304, 50mm in diameter and 10mm thick.

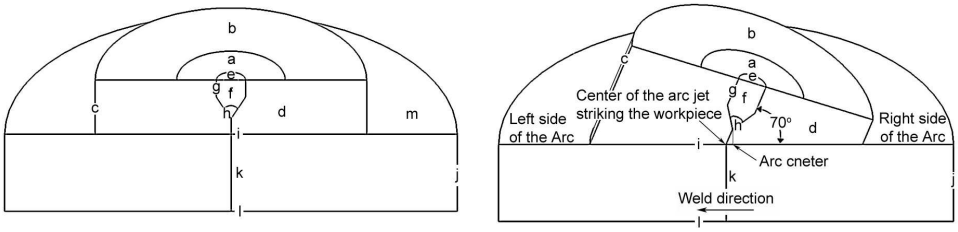

(a) (b)

Figure 1: Geometry for torch angles (a) 90^o (b) 70^o

2.3 Boundary conditions

2.3.1 The arc:

As temperature of the electrode cannot exceed the melting temperature, therefore it is set to 3000K. In Figure 1a, temperature at a, b and c boundaries is 303K. A current of 130A is applied at boundary e, the argon flow is set to 14 liter/min at boundary a. Magnetic induction is zero at boundary c. Boundary i is defined as fluid-solid interface between the arc and weld pool domains. Boundaries g and h are also fluid-solid interfaces between the arc and tungsten electrode domains. To simulate the effect of the tip angle, variable cathode lengths are used as given in reference (Haidar and Farmer, 1994). This approach gives different cathode surface areas for different tip angles surrounded by the plasma (boundary h in figure 1a). The part of the electrode not surrounded by the plasma is treated as fully insulated (boundary g in figure 1a). Symmetry boundary conditions are applied on boundaries d and f.

2.3.2 The weld pool:

Boundaries j, l and m are defined as wall with heat transfer coefficient of 20 W/m^2K. Boundary l is set to 0V. Boundary k is symmetric. The heat flux, current flux and gas shear stress are applied at boundary i . These boundary conditions are taken from the

Journal of Engineering Mechanics. Submitted May 20, 2011; accepted September 21, 2012;
posted ahead of print September 23, 2012. doi:10.1061/(ASCE)EM.1943-7889.0000553

steady state results of the arc. The Marangoni convection is calculated using equation 2 given in reference (Xu et al., 2007) and is added to the gas shear stress on boundary i.

$$\tau_x = \frac{\partial \gamma}{\partial T}\frac{\partial T}{\partial x}, \quad \tau_y = \frac{\partial \gamma}{\partial T}\frac{\partial T}{\partial y} \tag{2}$$

The temperature dependent surface tension is calculated using equation 3. Data for the calculation is taken from reference (Goodarzi et al., 1998).

$$\gamma(T) = \gamma_m - A_\gamma(T - T_m) - RT\Gamma_s ln(1 + Ka_i) \tag{3}$$

Where

$$K = k_1 exp(-\frac{\triangle H_o}{RT}) \tag{4}$$

2.4 Computational aspects

To ensure the mesh independency on the results, mesh sensitivity analysis is performed for the heat flux and gas shear stress and the same mesh size is then used for other studies. These two parameters are responsible for the weld pool calculation. The analysis is performed on Core i7 (8 CPUs) system with 2.80 GHz clock speed and 6.0 GB RAM. The change in values of the selected parameters is negligible after mesh size of 0.1mm and is therefore selected for analysis. The grid system is hexahedral and other computational information are given in figure 2.

Journal of Engineering Mechanics. Submitted May 20, 2011; accepted September 21, 2012;
posted ahead of print September 23, 2012. doi:10.1061/(ASCE)EM.1943-7889.0000553

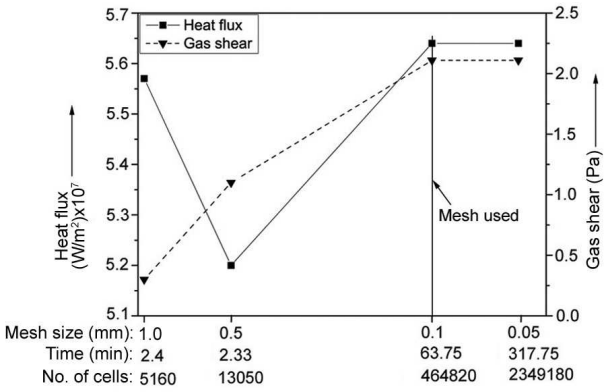

Figure 2: Mesh sensitivity results

3 Model validation

The two-dimensional model is validated with the available results of reference (Lowke et al., 1997) and is shown in figure 3. The welding current is 200A, electrode diameter is 3.2mm and the arc length is 5mm. The electrode tip angle is 60^o and the workpiece material is water cooled copper. Close agreement is observed in the isotherms of the arc and the weld pool. The two-dimensional model is then extended to three-dimension and is validated through experiments which is discussed in section *Experimental validation*.

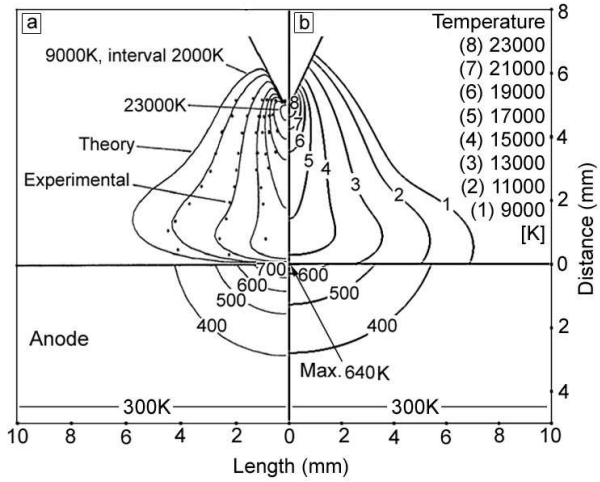

Figure 3: Comparison of arc temperatures (a) Lowke et al. (b) present study

Journal of Engineering Mechanics. Submitted May 20, 2011; accepted September 21, 2012;
posted ahead of print September 23, 2012. doi:10.1061/(ASCE)EM.1943-7889.0000553

4 Results and discussions

4.1 The arc temperature

The typical arc temperatures are observed symmetric for 90^o torch angle (figure 4a), whereas are non-symmetric for 70^o torch angle (figure 4b). The maximum arc temperature near the electrode tip is in the range of 17000K which shows close agreement with the calculated arc temperatures of reference (Shinichi et al., 2005). Tilting the torch from 90^o to 70^o increases the temperature distribution on the anode surface ahead of the electrode tip. The anode surface is the workpiece surface in the plasma arc region. Two reference temperatures, 7000K and 13300K are considered for comparison in figure 5. The latter is the maximum temperature on the anode surface which shifts about 0.2mm ahead of the arc center. The temperature distribution is the same across the weld direction. It shows that tilting the torch 70^o enlarges the heating zone in the weld direction. The temperature contour of 7000K shows about 2.2mm increase ahead and 1.4mm decrease behind the electrode tip as compared to 90^o torch.

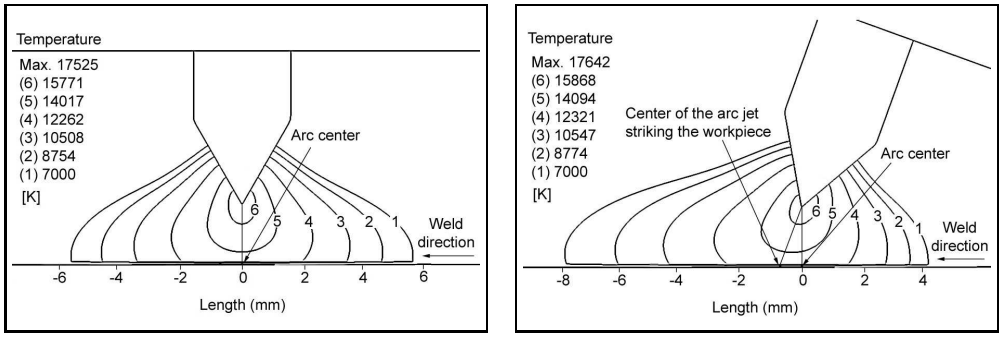

(a) (b)

Figure 4: Temperature in the arc column for torch angles (a) 90^o (b) 70^o

Journal of Engineering Mechanics. Submitted May 20, 2011; accepted September 21, 2012;
posted ahead of print September 23, 2012. doi:10.1061/(ASCE)EM.1943-7889.0000553

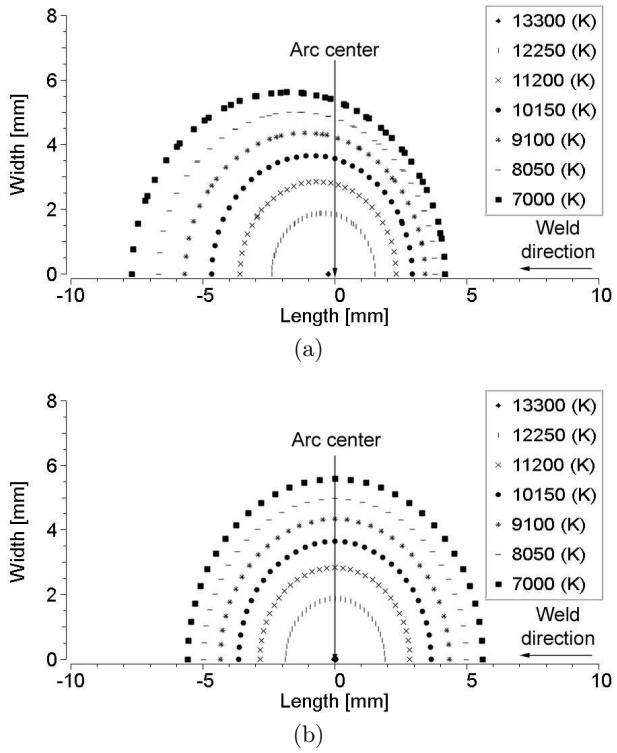

Figure 5: Contours of temperature on the anode surface (a) 90^o(b) 70^o

4.2 The arc velocity

The arc velocity in the arc column and on the workpiece surface is shown in figure 6 and figure 7 respectively which is symmetric for 90^o and non-symmetric for 70^o torch angle. The arc velocity is observed large for 70^o torch as compared to 90^o torch i.e, 142 m/s and 138 m/s in the arc column and 50 m/s and 29 m/s on the anode surface respectively. Moreover, in 90^o torch, the arc velocity is the minimum at the weld center, increasing to the maximum at about 1.5mm away from the weld center and then symmetrically decreasing to the minimum away from the arc center (figure 7a). In 70^o torch, the maximum velocity is also observed at about 1.5mm ahead of the electrode tip in the welding direction. The minimum contour of 7.6 m/s is compared which shows large distribution ahead and minimum distribution behind the electrode tip for 70^o as compared to 90^o torch angle.

Journal of Engineering Mechanics. Submitted May 20, 2011; accepted September 21, 2012;
posted ahead of print September 23, 2012. doi:10.1061/(ASCE)EM.1943-7889.0000553

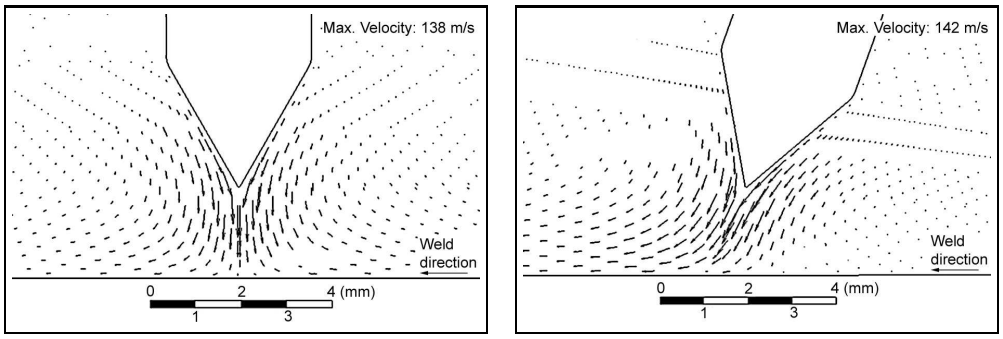

(a) (b)

Figure 6: Velocity flow patterns in the arc column for torch angles (a) 90^o(b) 70^o

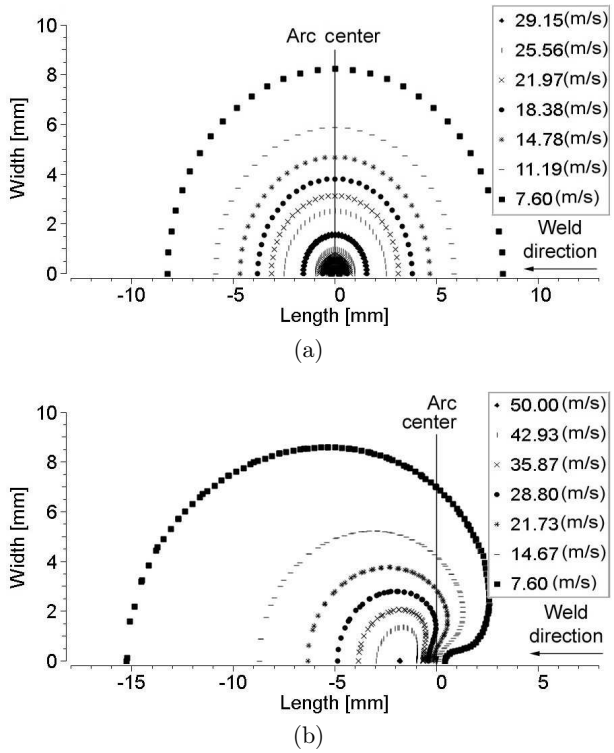

(a)

(b)

Figure 7: Contours of velocity on the anode surface for torch angles (a) 90^o(b) 70^o

4.3 The current density

Current density in the arc column is observed the maximum near the electrode tip in both the torch positions. For 70^o torch, the maximum current density is slightly larger than the 90^o torch; it is because more electrode tip area is exposed to the workpiece surface which increases the current density. The contours of current density distribution

Journal of Engineering Mechanics. Submitted May 20, 2011; accepted September 21, 2012;
posted ahead of print September 23, 2012. doi:10.1061/(ASCE)EM.1943-7889.0000553

on the anode surface are shown in figure 8. The distribution is symmetric for 90^o and is non-symmetric for 70^o torch position. The maximum current density of 6.3E6 A/m^2 is shifted about 0.5mm behind the arc center for 70^o torch. It is because more electrode tip area is exposed to the workpiece surface as compared to the other side. The current density of 1.00E6 A/m^2 is wider ahead of the arc center because less electrode tip area is exposed to the workpiece surface. The asymmetry in current density is observed less as compare to the temperature and velocity.

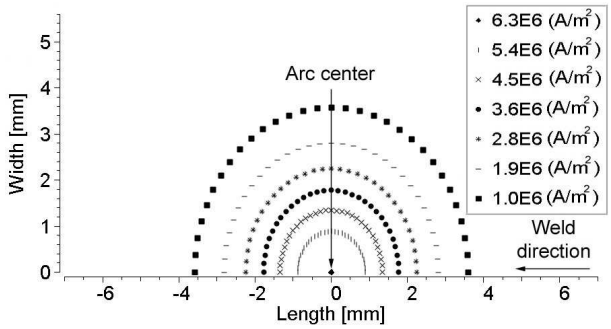

(a)

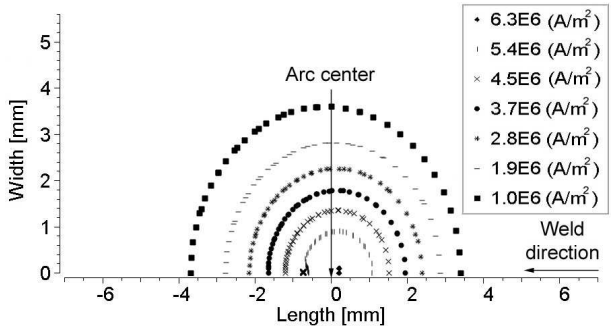

(b)

Figure 8: Contours of current density on the anode surface for torch angles (a) 90^o (b) 70^o

4.4 The heat flux

Heat flux determines the weld pool shape. Increasing the heat flux increases both the width and depth of the weld pool (Goodarzi et al., 1998). The two mechanisms of heat transfer to the workpiece in this model are the conduction/convection and electron contribution. Contours of heat flux due to conduction and convection are shown in figure 9. The distribution is symmetric for 90^o torch angle (figure 9a). For 70^o torch angle, the

Journal of Engineering Mechanics. Submitted May 20, 2011; accepted September 21, 2012;
posted ahead of print September 23, 2012. doi:10.1061/(ASCE)EM.1943-7889.0000553

distribution is non-symmetric and the maximum heat flux of 11.30E6 W/m^2 is 0.4mm ahead of the arc center and is at the center of the arc jet striking the workpiece (figure 9b). Also the heat flux due to conduction and convection is observed small in case of 70^o torch, it is because the arc velocity is large which decreases the heat flux at the surface of the workpiece due to cooling.

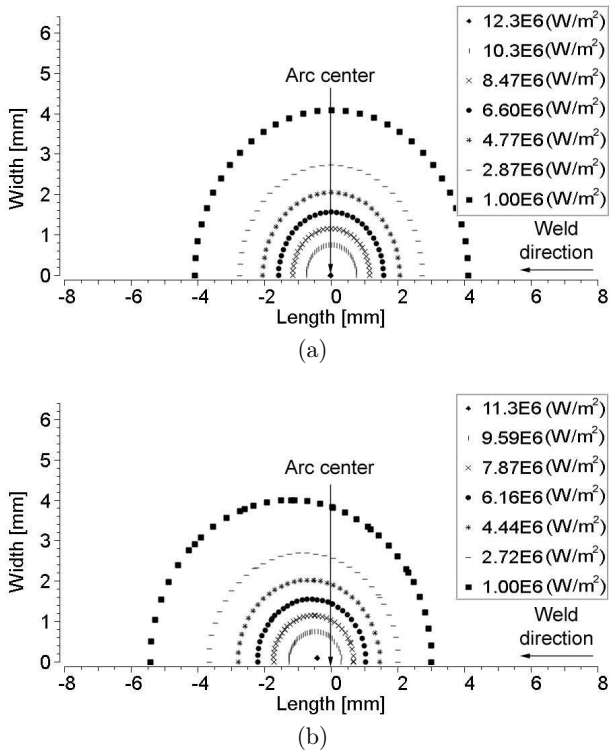

Figure 9: Contours of heat flux due to conduction and convection for torch angles (a) 90^o (b) 70^o

The total heat flux is calculated using equation 1 which is symmetric for 90^o torch angle. For 70^o torch angle, the distribution becomes almost symmetric for large value; however for small values, the contours are more ahead of the arc center due to torch angle. The distribution of minimum heat flux of 1.00E6 W/m^2 in 70^o torch is observed about 1.6mm large ahead and 1.1mm less behind the weld center as compared to the 90^o torch. The maximum heat flux is found at the arc center for both the torch positions. The distribution is observed the same across the weld direction.

Journal of Engineering Mechanics. Submitted May 20, 2011; accepted September 21, 2012;
posted ahead of print September 23, 2012. doi:10.1061/(ASCE)EM.1943-7889.0000553

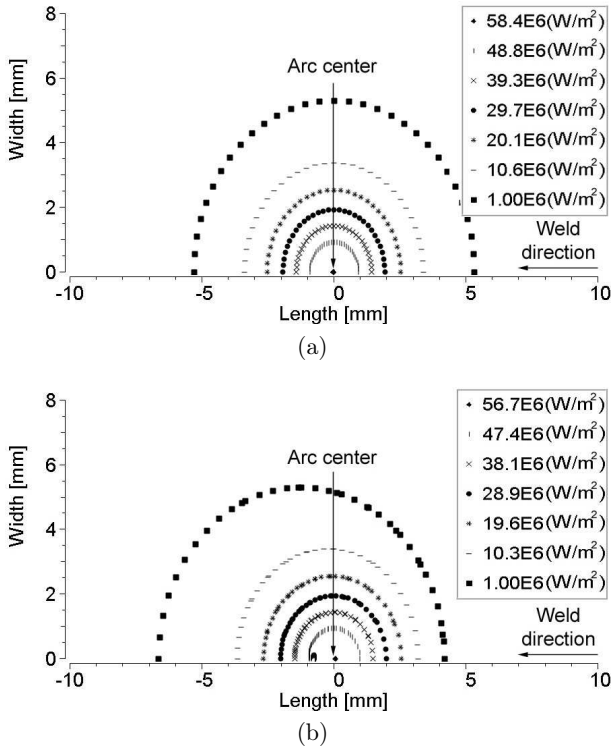

Figure 10: Contours of total heat flux on the anode surface for torch angles (a) 90^o (b) 70^o

4.5 The gas shear stress

The gas shear stress significantly alters the weld pool shape. Increasing the gas shear stress increases the width and decreases the depth of the weld pool. Figure 11 illustrates the distribution of the gas shear stress on the anode surface. The gas shear is determined primarily from the arc velocity (Westhoff, 1989), the distribution is therefore similar to the velocity of figure 7b. The gas shear stress is symmetric for 90^o torch angle. For 70^o torch angle, the direction of the gas shear is in the direction of the torch and is more ahead of the electrode tip. This action slightly shifts the weld pool ahead of the electrode tip in the weld direction. Since the arc velocity is large, the gas shear is also large in 70^o which develops weld pool of lesser depth as compared to the 90^o torch.

Journal of Engineering Mechanics. Submitted May 20, 2011; accepted September 21, 2012;
posted ahead of print September 23, 2012. doi:10.1061/(ASCE)EM.1943-7889.0000553

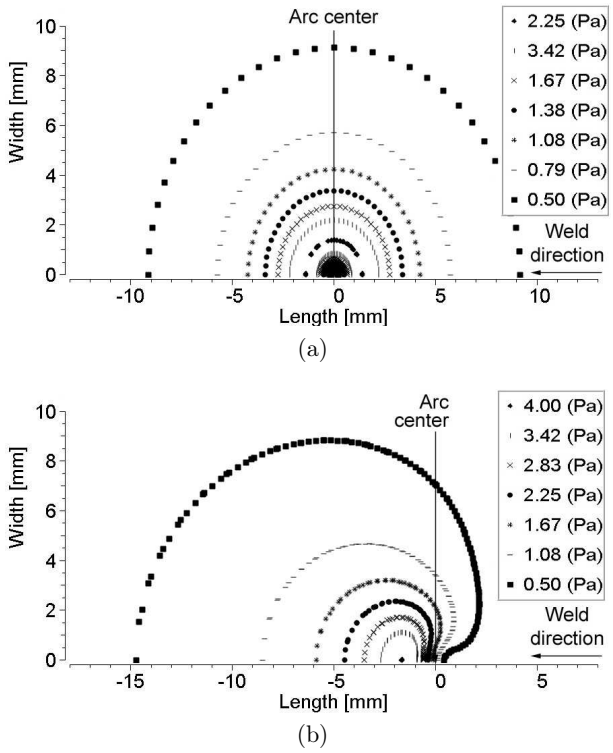

Figure 11: Contours of gas shear stress on the anode surface for torch angles (a) 90^o (b) 70^o

4.6 The Electromagnetic force

Figure 12a and figure 12b show the distribution of the electromagnetic force in the cross-section and at the top of the weld pool for 90^o and 70^o torch angles respectively. The electromagnetic force is symmetric for 90^o torch angle. The maximum force of 11.6E4 N/m^3 is observed at a distance of about 1.8mm from the weld center. The force decreases to 775 N/m^3 at the center of the weld. For 70^o torch, the force is non-symmetric and the largest force of 13.8E3 N/m^3 is found about 2mm behind the weld center in the weld direction. This is because, the electromagnetic force is calculated directly from the current density applied, and since the current density is large, the electromagnetic force is also large behind the weld center. Similarly, the distribution of the minimum force of 1.00E3 N/m^3 is observed about 0.5mm ahead in the welding direction for 70^o as compared to 90^o torch.

Journal of Engineering Mechanics. Submitted May 20, 2011; accepted September 21, 2012;
posted ahead of print September 23, 2012. doi:10.1061/(ASCE)EM.1943-7889.0000553

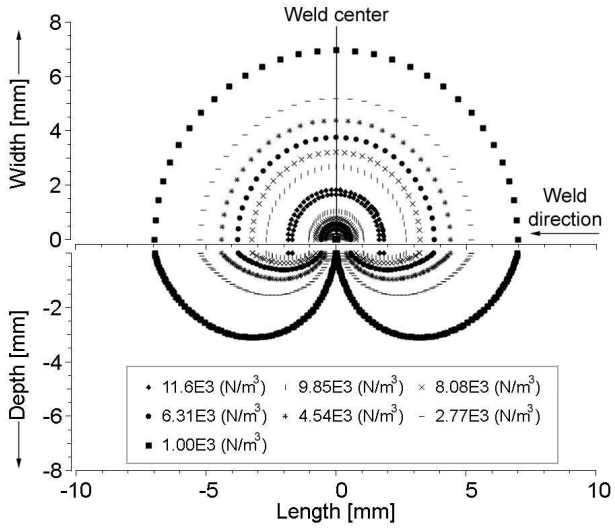

(a)

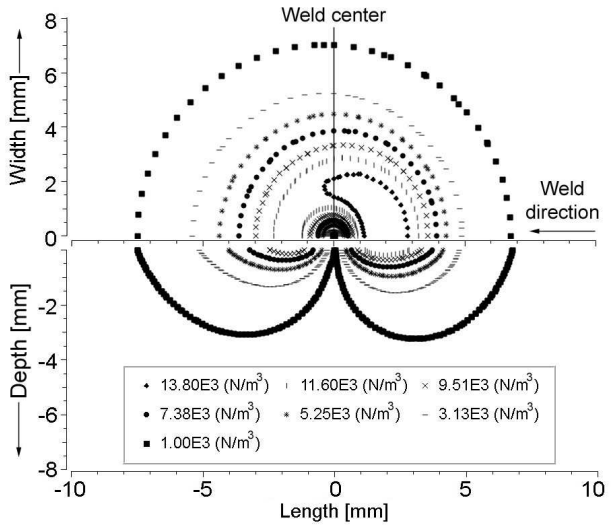

(b)

Figure 12: Contours of the electromagnetic force in the weld pool for torch angles (a) 90^o (b) 70^o

4.7 Buoyancy force in the weld pool

The buoyancy force is large where the temperature is large as shown in figure 13. Figure 13a and figure 13b represents the symmetric and non-symmetric distributions of buoyancy force for 90^o and 70^o torch angles respectively. For 90^o torch angle, the temperature is maximum at the weld center resulting in large buoyancy force. On the other hand, due to *"w"* weld pool shape, buoyancy force is also large away from the arc center. In 70^o torch (as

Journal of Engineering Mechanics. Submitted May 20, 2011; accepted September 21, 2012;
posted ahead of print September 23, 2012. doi:10.1061/(ASCE)EM.1943-7889.0000553

compared to 90^o torch), the maximum buoyancy force of 4.72E3 N/m^3 is observed about 1.3mm behind the weld center. Similarly the distribution of the minimum buoyancy force of 20 N/m^3 is observed about 0.9mm ahead and 0.6mm behind in the weld direction for 70^o as compared to 90^o torch.

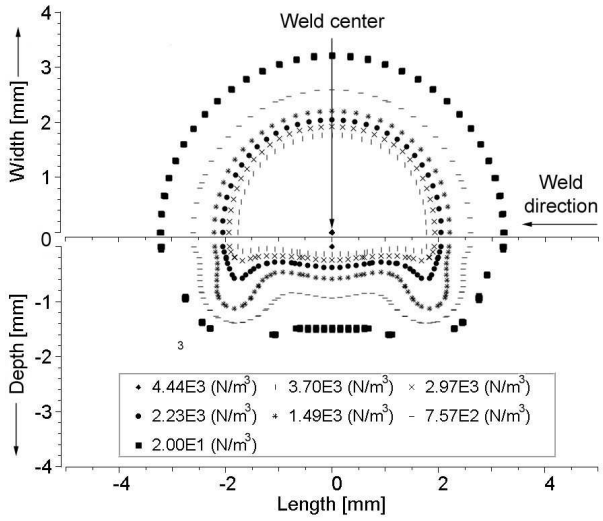

(a)

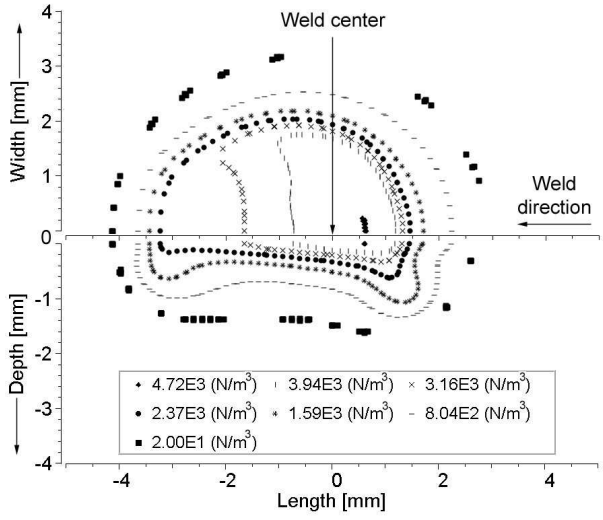

(b)

Figure 13: Contours of the buoyancy force in the weld pool for torch angles (a) 90^o (b) 70^o

Journal of Engineering Mechanics. Submitted May 20, 2011; accepted September 21, 2012;
posted ahead of print September 23, 2012. doi:10.1061/(ASCE)EM.1943-7889.0000553

4.8 Convection in the weld pool

Velocity vectors in the cross-section and at the top of the weld pool are shown in figure 14 and in figure 15 respectively. The sign of the surface tension gradient ($\frac{\partial \gamma}{\partial T}$) determines the flow direction on the weld pool surface. The fluid flows away from the center of the weld pool where the sign of the Marangoni convection and the gas shear is positive and is directed towards the center of the weld pool where it is negative. A *"w"* shaped weld pool is produced when the flow is both positive and negative. The contribution of buoyancy and electromagnetic force is minor in the weld pool convection (Goodarzi et al., 1998). For 70^o as compared to 90^o torch angle, the convection is large at the surface of the workpiece and is observed in the direction of the torch (figure 15b). The weld pool width is therefore large ahead of the electrode tip.

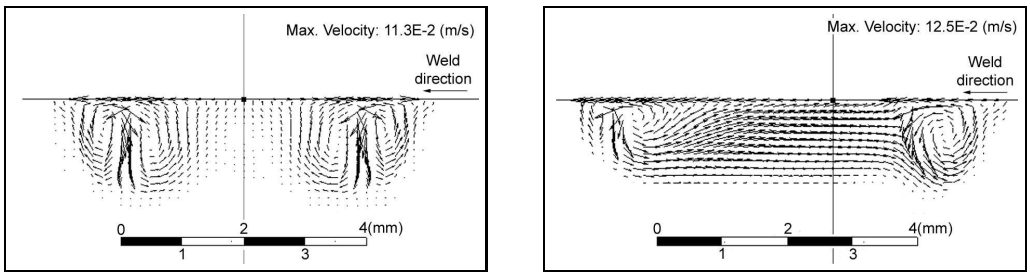

(a) (b)

Figure 14: Fluid flow in the cross-section of the weld pool for torch angles (a) 90^o (b) 70^o

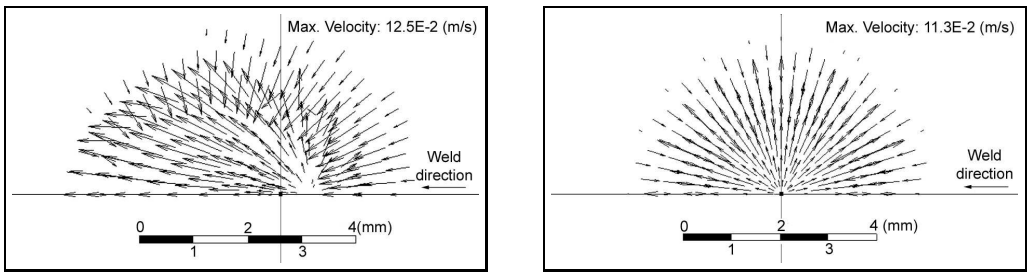

(a) (b)

Figure 15: Fluid flow at the top of the weld pool for torch angles (a) 90^o (b) 70^o

Journal of Engineering Mechanics. Submitted May 20, 2011; accepted September 21, 2012;
posted ahead of print September 23, 2012. doi:10.1061/(ASCE)EM.1943-7889.0000553

4.9 The weld pool

A comparison of the weld pool width and depth is shown in figure 16. Figure 16a represents the weld pool width on the top surface of the workpiece. It is found that for 70^o torch, the weld pool is asymmetric, wide in the weld direction and shallow as compared to the 90^o torch angle. Figure 16b shows that the width is small and depth is large behind the weld center as compared to the other side. It is because the effect of gas shear stress is small and Marangoni convection is large behind the weld center (depicted by the velocity vectors towards the center of the arc in figure 15b) and is otherwise on the other side. This phenomenon decreases the width and increases the depth behind and increases the width and decreases the depth ahead of the weld center. Overall, the weld pool is about 1.8mm deep in both the torch positions; however, is wide about 6.5mm in 90^o and 7mm in 70^o torch positions. The weld pool is observed to shift about 0.25mm ahead of the electrode tip along the weld direction. The width of pool remains unaffected across the weld direction.

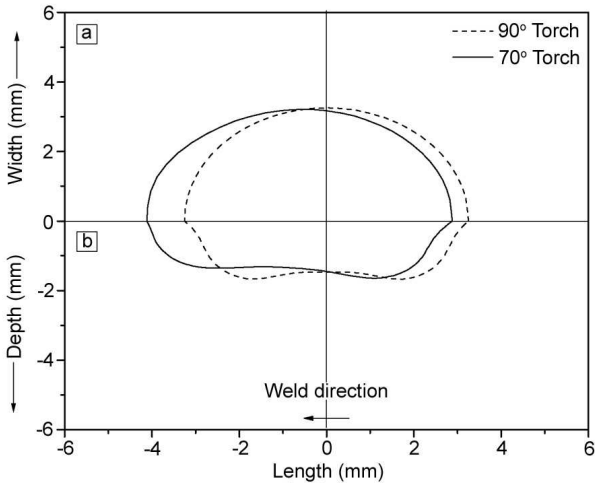

Figure 16: Weld pool shapes (a) width (b) depth

5 Experimental validation

Figure 17 and figure 18 present a comparison between the numerically and experimentally determined weld pool width and depth respectively and are observed in good agreement.

Journal of Engineering Mechanics. Submitted May 20, 2011; accepted September 21, 2012;
posted ahead of print September 23, 2012. doi:10.1061/(ASCE)EM.1943-7889.0000553

The weld pool is wide ahead of the electrode tip in the weld direction for 70^o torch angle as shown in figure 20b which is consistent with the numerical results.

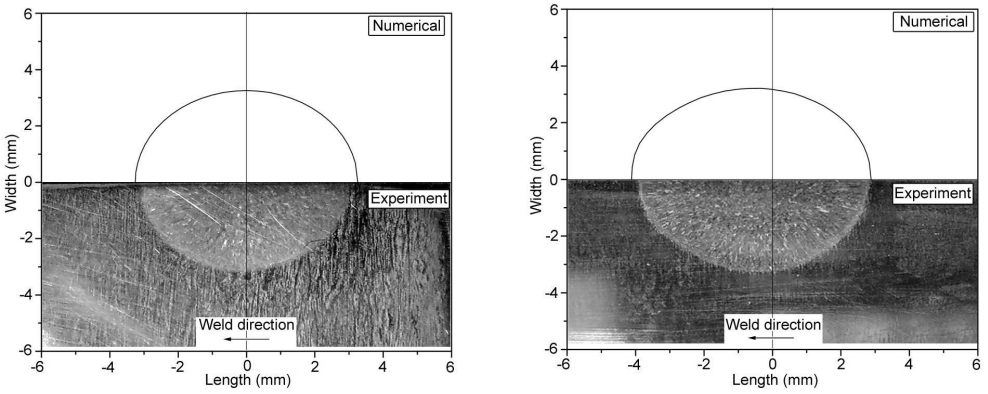

(a) (b)

Figure 17: Weld pool width on top of the workpiece for torch angles (a) 90^o (b) 70^o

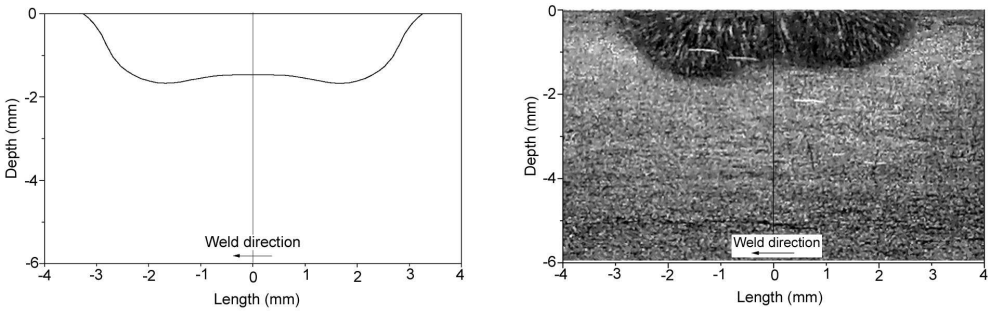

(a) (b)

Figure 18: Weld pool depth for 90^o torch (a) Numerical (b) Experimental

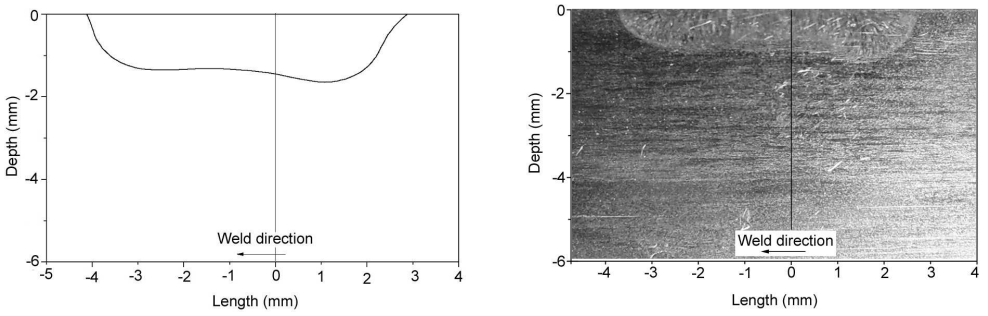

(a) (b)

Figure 19: Weld pool depth for 70^o torch (a) Numerical (b) Experimental

Journal of Engineering Mechanics. Submitted May 20, 2011; accepted September 21, 2012;
posted ahead of print September 23, 2012. doi:10.1061/(ASCE)EM.1943-7889.0000553

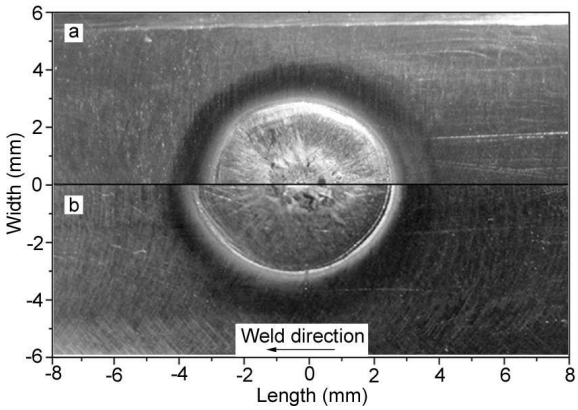

Figure 20: Experimental weld pool width for torch angles (a) 90^o (b) 70^o

6 Conclusions

A three dimensional model for the GTAW is developed to investigate the effect of torch angle on the arc and weld pool properties. The arc is solved in steady state and the weld pool is solved for two seconds. To evaluate the relative distribution of current density, heat flux, gas shear stress, buoyancy and weld pool shape, each parameter is compared for 90^o and 70^o torch positions. For 90^o torch angle, both the arc and weld pool are symmetric. For 70^o torch angle, the distribution of the current density and hence the heat flux due to electron contribution is more behind the arc center in the weld direction. On the other hand, heat flux due to conduction and convection is more ahead of the arc center. This makes the total heat flux symmetric for large values. However for small values, the distribution of the heat flux is more ahead of the arc center. It is found that the heat flux due to conduction and convection is sensitive to the torch angle and decreases as the torch angle decreases.

The electromagnetic force is calculated from the current density and is large behind the weld center for 70^o torch angle. The fluid flow in the weld pool is primarily determined by the gas shear and Marangoni convection. The change in sign of $\frac{\partial \gamma}{\partial T}$ develops the *"w"* shape weld pool and consequently the depth for 70^o torch angle is large behind and small and wide ahead of the arc center. No change in the pool width is observed across the weld direction. It can be concluded that for the torch angles less than 90^o, the weld pool

Journal of Engineering Mechanics. Submitted May 20, 2011; accepted September 21, 2012; posted ahead of print September 23, 2012. doi:10.1061/(ASCE)EM.1943-7889.0000553

becomes asymmetric, shallow and wide ahead of the electrode tip in the weld direction. Good agreement is observed between the numerical and experimental weld pool shapes.

Nomenclature

A_γ	Temperature coefficient of surface tension for iron $(4.3 \times 10^{-4} N/mK)$
a_i	The activity of sulfur (0.022 wt%)
F	Total heat flux (W/m^2)
F_c	Heat flux due to conduction and convection (W/m^2)
j	Current density (A/m^2)
k_1	The entropy factor (0.00318 $\text{wt\%}^{-1}$)
R	Gas constant $(8.3144\, J/molK)$
T	Temperature (K)
T_m	Melting temperature of iron in equation 3 $(1800K)$
V_a	Anode fall voltage $(2V)$
V_{th}	Equivalent volt drop at the anode $(1V)$
$\triangle H_o$	Enthalpy of segregation $(-1.88 \times 10^5 J/mol)$
Γ_s	The surface excess at saturation $(1.3 \times 10^{-5} mol/m^2)$
ϕ	Workfunction $(4.3V)$
γ	Surface tension (N/m)
γ_m	Surface tension of iron at T_m $(1.943\, N/m)$
τ_x	Marangoni convection x component (Pa)
τ_y	Marangoni convection y component (Pa)

Journal of Engineering Mechanics. Submitted May 20, 2011; accepted September 21, 2012; posted ahead of print September 23, 2012. doi:10.1061/(ASCE)EM.1943-7889.0000553

References

ANSYS (2010). "ANSYS CFX®, Academic Research, Release 13.0, Help system, ANSYS CFX-Solver theory guide, ANSYS, Inc.

Choo, R. T. C., Szekely, J., and David, S. A. (1992). "On the calculation of the free surface temperature of Gas-Tungsten-Arc weld pools from first principles: Part II. Modelling the weld pool and comparison with experiments." *Metallurgical Transactions B*, 23B, 371–384.

Ferjutz, K. and Davis, J. R. (1993). "ASM Handbook: Welding, brazing and soldering." Vol. 6, ISBN: 0871703823.

Gleizes, A., Bouaziz, M., Gonzalez, J. J., and Razafinimanana, M. (1997). "Influence of the anode material on an argon arc." *IEEE Transaction on Plasma Science*, 25(5), 891–896.

Gleizes, A., Gonzalez, L. L., and Freton, P. (2005). "Thermal plasma modeling." *J. Phys. D: Appl. Phys.*, 38, R153–R183.

Gonzalez, J. J., Lago, F., Freton, P., Masquere, M., and Franceries, X. (2005). "Numerical modeling of an electric arc and its interaction with the anode: Part II. The three-dimensional model-influence of external forces on the arc column." *J. Phys. D: Appl. Phys.*, 38, 306–318.

Goodarzi, M., Choo, R., Takasu, T., and Toguri, J. M. (1998). "The effect of the cathode tip angle on the gas tungsten arc welding arc and weld pool: II. The mathematical model for the weld pool." *J. Phys. D: Appl. Phys.*, 31, 569–583.

Haidar, J. and Farmer, A. J. D. (1994). "Large effect of cathode shape on plasma temperature in high-current free-burning arcs." *J. Phys. D: Appl. Phys.*, 27, 555–560.

Kanouff, M. (1992). "The unsteady development of a GTA weld pool." *Int. J. Heat Mass transfer*, 35, 967–979.

Journal of Engineering Mechanics. Submitted May 20, 2011; accepted September 21, 2012; posted ahead of print September 23, 2012. doi:10.1061/(ASCE)EM.1943-7889.0000553

Kim, W. H. and Na, S. J. (1998). "Heat and fluid flow in pulsed current GTA weld pool." *Int. J. Heat Mass transfer*, 41, 3213–3227.

Leibowitz, L. (1976). "Properties for LMFBR safety analysis." *Report No. ANL-CEN-RSD-76-1*, Argonne National Laboratories.

Li, Z. Y. and Wu, C. S. (1997). "Analysis of the transport phenomena in the interfacial region between TIG arcs and weld pools." *Computational Materials Science*, 8, 243–250.

Lowke, J. J., Morrow, R., and Haidar, J. (1997). "A simplified unified theory of arcs and their electrodes." *J. Phys. D: Appl. Phys.*, 30, 2033–2042.

Lu, F., Tang, X., Yu, H., and Yao, S. (2006). "Numerical simulation on interaction between TIG welding arc and weld pool." *Computational Materials Science*, 35, 458–465.

Lu, F., Yau, S., Lou, S., and Li, Y. (2004). "Modeling and finite element analysis on GTAW arc and weld pool." *Computational Materials Science*, 29, 371–378.

Miller (2008). "Guidelines for Gas Tungsten Arc Welding (GTAW).

Murphy, A. B. and Arundell, C. J. (1994). "Transport coefficients of Argon, Nitrogen, Oxygen, Argon-Nitrogen, and Argon-Oxygen plasmas." *Plasma Chemistry and Plasma Processing*, 14, 451–490.

Quigley, M. B. C., Richards, P. H., Swift-Hook, D. T., and Gick, A. E. F. (1973). "Heat flow to the workpiece from a TIG welding arc." *J. Phys. D: Appl. Phys.*, 6, 2250–2258.

Sansonnens, L., Haidar, J., and Lowke, J. J. (2000). "Prediction of properties of free burning arcs including effect of ambipolar diffusion." *J. Appl. Phys.*, 33, 148–157.

Shinichi, T., Manbu, T., and Masao, U. (2005). "Numerical simulation of GTAW in different gaseous atmospheres." *Transactions of JWRI*, 34(2), 1–5.

Journal of Engineering Mechanics. Submitted May 20, 2011; accepted September 21, 2012; posted ahead of print September 23, 2012. doi:10.1061/(ASCE)EM.1943-7889.0000553

Speckhofer, G. and Schmidt, H.-P. (1996). "Experimental and theoretical investigation of high-pressure arcs-Part II: The magnetically deflected arc (Three-dimensional modeling)." *IEEE Transaction on Plasma Science*, 24, 1239–1248.

Tanaka, M., Terasaki, H., Ushio, M., and Lowke, J. J. (2002). "A unified numerical modeling of stationary tungsten inert gas welding process." *Metallurgical and Materials Transactions*, 33A, 2043–2052.

Thompson, M. E. and Szekely, J. (1989). "The transient behavior of weldpools with a deformed free surface." *Int. J. Heat Mass transfer*, 32, 1007–1019.

Westhoff, R. C. (1989). "A mathematical model for current, heat flux and pressure in a welding arc." Ph.D. thesis, MIT Department of Material Science and Engineering, MIT Department of Material Science and Engineering.

Wu, C. S. and Gao, J. Q. (2002). "Analysis of the heat flux distribution at the anode of a TIG welding arc." *Computational Materials Science*, 24, 323–327.

Xu, Y. L., Dong, Z. B., Wei, Y. H., and Yang, C. L. (2007). "Marangoni convection and weld shape variation in A-TIG welding process." *Theoretical and Applied Fracture Mechanics*, 48, 178–186.

yun Du, H., hui Wei, Y., xian Wang, W., ming Lin, W., and Fan, D. (2009). "Numerical simulation of temperature and fluid in GTAW arc under changing process conditions." *Journal of Material Processing Technology*, 209, 3752–3765.

Zhu, P., Lowke, J. J., Morrow, R., and Haidar, J. (1995). "Prediction of anode temperatures of free burning arcs." *J. Appl. Phy.*, 28, 1369–1376.